Talanta 238 (2022) 123008

Contents lists available at ScienceDirect

Talanta

journal homepage: www.elsevier.com/locate/talanta

Simultaneous quantification of selected glycosaminoglycans by butanolysis-based derivatization and LC-SRM/MS analysis for assessing glycocalyx disruption *in vitro* and *in vivo*

Karolina Matyjaszczyk-Gwarda [a], Agnieszka Kij [a], Mariola Olkowicz [a], Benedikt Fels [b], Kristina Kusche-Vihrog [b], Maria Walczak [a,c], Stefan Chlopicki [a,d,*]

[a] Jagiellonian University, Jagiellonian Centre for Experimental Therapeutics (JCET), Bobrzynskiego 14, 30-348, Krakow, Poland
[b] Universität zu Lübeck, Institut für Physiologie, Ratzeburger Allee 160, Gebäude 61, D-23562, Lübeck, Germany
[c] Jagiellonian University Medical College, Chair and Department of Toxicology, Medyczna 9, 30-688, Krakow, Poland
[d] Jagiellonian University Medical College, Chair of Pharmacology, Grzegorzecka 16, 31-531, Krakow, Poland

ARTICLE INFO

Keywords:
Glycosaminoglycans
Glycocalyx
Butanolysis
Liquid chromatography-tandem mass spectrometry
Endothelium
Atherosclerosis

ABSTRACT

Glycosaminoglycans (GAGs) constitute the main building blocks of the endothelial glycocalyx (GLX), and disruption of GLX initiates and promotes endothelial dysfunction. Here, we aimed to develop a novel, specific and accurate LC-SRM/MS-based method for glycosaminoglycans (GAGs) profiling. The method involved butanolysis derivatization to facilitate GAG-specific disaccharide generation and its subsequent retention in LC–reversed-phase mode followed by mass spectrometric detection performed in positive ion-selected reaction monitoring (SRM) mode. GAG contents were measured in media of endothelial cells (EA.hy926) subjected to various GAG-degrading enzymes, as well as in murine plasma and urine in apolipoprotein E/low-density lipoprotein receptor-deficient (ApoE/LDLR −/−) mice and age-matched wild-type C57BL/6 mice. Alternatively, GLX disruption was verified by atomic force microscopy (AFM)-based analysis of GLX thickness. The proposed assay to quantify GAG-specific disaccharides presented high sensitivity for each of the analytes (LLOQ: 0.05–0.1 μg/mL) as well as accuracy and precision (86.8–114.9% and 2.0–14.3%, respectively). In medium of EA.hy926 cells subjected to GAG-degrading enzymes various GAG-specific disaccharides indicating the degradation of keratan sulphate (KS), heparan sulphate (HS), chondroitin sulphate (CHS) or hyaluronan (HA) were detected as predicted based on the characteristics of individual enzyme activity. In turn, AFM-based assessment of GLX thickness was reduced to a similar extent by all single enzyme treatments, whereas the most prominent reduction of GLX thickness was detected following the enzyme mixture. Plasma measurements of GAGs revealed age- and hypercholesterolemia-dependent decrease in GAGs concentration. In summary, a novel LC-SRM/MS-based method for GAG profiling was proposed that may inform on GLX status in cell culture for both *in vitro* and *in vivo* conditions.

1. Introduction

The endothelial glycocalyx (GLX)—a brush-like surface layer composed of proteoglycans and glycoproteins lining the luminal surface of the endothelium—plays an important role in maintaining endothelial integrity [1]. The loss of GLX integrity was suggested to initiate and promote endothelial dysfunction, which is characterized by increased vascular permeability, endothelial stiffness, activation of leukocytes adhesion and endothelial inflammation, activation of pro-thrombotic mechanisms of the endothelium and decreased NO production [2,3].

Interestingly, in recent years, a number of reciprocal mechanisms have been described suggesting feedback forward reinforcement mechanisms between perturbed endothelial GLX and endothelial dysfunction progression [4]. For example, the deterioration of GLX resulted in increased endothelial permeability and stiffness [5], whereas endothelial barrier disruption was linked to increased angiopoietin-2

Abbreviations: AFM, atomic force microscopy; CHS, chondroitin sulphate; DS, dermatan sulphate; GlcUA, D-glucuronic acid; GAGs, Glycosaminoglycans; GLX, glycocalyx; HS, heparan sulphate; HA, hyaluronan; IdoUA, L-iduronic acid; KS, keratan sulphate; PG, proteoglycan; SRM, selected reaction monitoring.

* Corresponding author. Jagiellonian Centre for Experimental Therapeutics (JCET), Bobrzynskiego 14, 30-348, Krakow, Poland.
E-mail address: stefan.chlopicki@jcet.eu (S. Chlopicki).

https://doi.org/10.1016/j.talanta.2021.123008
Received 3 August 2021; Received in revised form 26 October 2021; Accepted 27 October 2021
Available online 28 October 2021

that mediated GLX breakdown [6]. Furthermore, GLX shedding facilitates monocyte adhesion and infiltration that promotes vascular inflammation, lipid retention and the development of atherosclerotic plaques [7]. In turn, leukocyte infiltration and subsequent vascular inflammation promote extrinsic pathways of GLX degradation by various shedasses (e.g., heparinases, hyaluronidases and matrix metalloproteinases), activating endothelial inflammation as well as thrombotic and fibrinolytic processes [8]. Similarly, impaired endothelial GLX promotes platelet adhesion to the endothelium [9,10]. Altogether, GLX injury seems to contribute to the impairment of NO-dependent function, increased endothelial permeability and stiffness, vascular inflammation, thrombosis, fibrinolysis and atherosclerosis development, and all these processes may reciprocally promote further GLX injury. Of note, it was suggested that in some pathologies, GAGs are shed from the GLX earlier than their membrane-anchored proteoglycan (PG) ectodomains; thus, GAGs may represent early-stage biomarkers [11].

In our recent study, we demonstrated that pronounced GLX injury coincided with various manifestations of endothelial dysfunction occurring before atherosclerotic plaque development in ApoE/LDLR-/- mice. Biomarkers of GLX injury may, therefore, provide a reliable insight into early changes of endothelial phenotype [12]. A growing body of literature has investigated alternations in GLX, including GAG concentrations in different physiological and pathological states, such as sepsis [13,14], mucopolysaccharidosis [15], ischemic stroke [16] and severely injured trauma patients [17]. GLX degradation was also suggested to contribute to vascular dysfunction in various viral infections, including COVID-19 [18]. Most of these studies, however, provided only limited insight into the quite complex biochemical nature of GLX. Indeed, the proteoglycans of GLX are decorated with long, unbranched glycosaminoglycans (GAGs), including heparan sulphate (HS), chondroitin sulphate (CHS), keratan sulphate (KS) and hyaluronan (HA). Inasmuch as GAGs are highly heterogeneous polysaccharides composed of disaccharide subunits, often with complex sulfation or acetylation patterns, their quantification at physiological concentrations is challenging [19].

Furthermore, all GAGs, are structurally similar. Thus, HS contains either D-glucuronic acid (GlcUA) or L-iduronic acid (IdoUA), which may be O-2 sulphated. The hexosamine unit could be N-acetylated or N-sulphated D-glucosamine, which may be O-3 or O-6-sulphated [20]. CHS contains GlcUA, which may be O-2 sulphated and as a hexosamine unit D-N-acetylgalactosamine, which may be 4-O and/or 6-O sulphated. The only structural difference between CHS and DS is the presence of some IdoA in the latter [21,22]. In turn, HA consists of GlcUA and N-acetyl-D-glucosamine, and it is the only GAG that is exclusively non-sulphated [23]. KS comprises D-galactose and N-acetylglucosamine, which may be 6-*O*-sulphated [24]. These structural similarities make the individual quantification of the KS-, HS-, CHS- and HA-constituents of GLX rather challenging. Structures of studied GAGs are showed in Fig. 2.

Several attempts have been proposed for the qualitative and quantitative analysis of GAGs, including separation by paper or thin-layer chromatography, gas chromatography, capillary electrophoresis, enzyme-linked immunosorbent assay and high-performance liquid chromatography [25]. The main disadvantages of the currently used techniques/methods include low sensitivity, incomplete chromatographic separation and co-elution of GAGs with other endogenous compounds.

Most of the methods used so far to assess GLX, characterize glycocalyx structure or biochemical content, rather than its function. Interestingly, DNA-origami-based nanosensors to monitor GLX integrity during pathophysiological processes have been recently proposed [26]. This novel method is aimed to assess glycocalyx barrier integrity and could well be used for the functional characterization of GLX and represents an interesting novel tool in glycocalyx research, enlarging the existing methodology of AFM, TEM and multiple analytical methods currently used to assess the GLX. Unfortunately DNA-origami-based nanosensors could not be used *in vivo*, in contrast to analytical methods to measure GAGs in plasma.

Among analytical methods, the LC-MS/MS based approach is superior in accuracy, speed, sensitivity, and specificity to previously proposed methods [26]. A properly developed methodology allows the detection of individual GAG in one run, which is a huge advantage in comparison to colorimetric methods which are generally used to quantify total GAG amount and concurrently led to a high number of false-positives and false-negative results [27,28]. LC-MS/MS based approach can also overcome the main disadvantages of commercially available ELISA kits, which include quantification of only one analyte at a time and cross-reactivity of antibodies. Furthermore, LC-MS/MS method requires low volume of samples to perform the analysis as compared to other methods [29].

Herein, we proposed a new LC-SRM/MS-based method for the simultaneous quantification of selected GAG disaccharides representing degradation products of the KS-, HS-, CHS- and HA-constituents of GLX. Based on this method, we demonstrated distinct changes in GLX degradation profile by various GAG-degrading enzymes in endothelial cells *in vitro* as well as a distinct age-dependent changes of GLX degradation profile in C57BL/6 and ApoE/LDLR−/− mice *in vivo*.

2. Materials and methods

2.1. Chemicals and reagents

Heparin sodium salt, chondroitin sulphate B sodium salt (dermatan), chondroitin sulphate sodium salt and hyaluronic acid sodium salt were bought from Sigma Aldrich (St. Louis, Missouri, USA). Sodium keratan sulphate was obtained from Amsbio (Abingdon, UK). The solution of 3 M hydrochloric acid in methanol and butanol, sodium chloride, ammonium acetate, formic acid, metoprolol, penicillin, streptomycin, HAT media supplement, heparinases I, II, III, endo-β-galactosidase, hyaluronidase and chondroitinase ABC were purchased from Sigma-Aldrich (St. Louis, Missouri, USA). DMEM medium and foetal bovine serum were purchased from Thermo Scientific (Warsaw, Poland). Ethanol, chloroform and LC/MS grade acetonitrile were bought from Witko (Lodz, Poland). Ultrapure water was obtained directly from a Milli-Q water purification system (Merck, Darmstadt, Germany).

Artificial plasma was prepared according to European Standard EN ISO 10993–15:2009. To 0.5 L of ultrapure water, 3.4 g of NaCl, 0.1 g of $CaCl_2$, 0.2 g of KCl, 0.05 g of $MgSO_4$, 1.1 g of $NaHCO_3$, 0.08 g of $Na_2HPO_4x2H_2O$ and 0.01 g of NaH_2PO_4 were mixed until all crystals were dissolved. Then, the correct amount of albumin was added to obtain the final physiological concentration of proteins (ca. 60 g/L). The artificial plasma pH was 7.35–7.45.

Artificial urine was prepared using 1 L of ultrapure water as previously reported and contained the following salts: 24.2 g of urea, 10.0 g of NaCl, 6.0 g of KCl, 6.4 g of Na_2HPO_4 and 2.0 g of creatinine. Then, the correct amount of albumin was added, obtaining the physiological concentration of proteins (ca. 0.05 g/L). The artificial urine pH was 5–7.

The pH of the artificial biofluids was adjusted with 1 M HCl or 1 M NaOH. Artificial biofluids without albumin addition were stored at 4 °C. The correct amount of albumin was mixed with artificial plasma or urine on the day of sample preparation. All salts necessary for artificial plasma preparation were delivered by Sigma Aldrich (St. Louis, Missouri, USA) or Avantor (Radnor, Pennsylvania, USA).

2.2. Preparation of stock solutions, calibration curves and quality control samples

Stock solutions of KS, CHS, HA, HS and DS at a concentration of 5 mg/mL were prepared in water and stored in aliquots at −20 °C until use. Target analyses were conducted using calibration curves covering a concentration range from 0.05 to 80 μg/mL. Quality control (QC) samples were prepared at three different concentrations: low (0.6 μg/mL), medium (40 μg/mL) and high (60 μg/mL).

Table 1
Mass spectrometry parameters for the quantitative analysis of disaccharides obtained after the butanolysis of DS, HS, CS, KS and IS.

GAGs	Q1 [m/z]	Q3 – quan		Q3 – qual		t_R [min]	Tube lens [V]
		[m/z]	CE [eV]	[m/z]	CE [eV]		
KS	398.2	162.0	14	84.0	14	1.39	90
CHS	468.2	162.0	20	394.0	20	5.77	80
HA	468.2	394.0	13	162.0	13	6.51	90
HS	468.2	162.0	20	394.0	20	10.36	80
IS	268.2	191.1	20	159.1	20	4.89	95

CE – collision energy; t_R-retention time.

The solution of metoprolol used as the internal standard (IS) at a concentration of 10 μg/mL was prepared in water and stored in aliquots at −20 °C until use.

2.3. Sample preparation

Calibration curves, QC samples and examined samples were treated with the same procedure. To precipitate proteins, 20 μL of 4 M NaCl was added to 50 μL of sample. After boiling for 10 min (100 °C), the sample was cooled to room temperature for 10 min, and then 50 μL of chloroform was added to remove plasma lipids. The samples were vortexed for 5 min and centrifuged at 12 000×*g*, 4 °C for 10 min. Then, 50 μL of supernatant was collected, and 150 μL of ethanol was added. The solution was kept at −80 °C for 15 min for GAG precipitation. The precipitate was recovered by centrifugation at 2000×*g*, 4 °C for 10 min and dried at 47 °C under a nitrogen stream. The dried residue was dissolved in 100 μL of water by prolonged mixing and after centrifugation (8000×*g*, 4 °C, 10 min) to remove insoluble interferences, it was transferred to glass tubes and freeze-dried overnight to completely remove water for efficient butanolysis. The application of freeze-drying instead of drying under a nitrogen stream at this stage allowed to eliminate the use of additional hygroscopic chemicals such as 2,2-dimethoxypropane which can result in creating colourful products of condensation [30]. The samples were derivatized by adding 100 μL of 3 M HCl in butanol. Samples were closely sealed, mixed (5 min) and then incubated at 100 °C for 30 min. After incubation, the samples were dried under nitrogen at 47 °C and then reconstituted in 50 μL of ACN:H_2O (1:1 v/v), and 5 μL of IS (10 μg/mL) was added.

During the development of the most suitable and efficient procedure for sample preparation, derivatization by methanolysis was also performed. The sample preparation procedure was the same as for butanolysis, except for the temperature of incubation, which was performed at 65 °C.

2.4. LC-MS/MS conditions

2.4.1. Chromatography

Chromatographic separation was performed using an UltiMate 3000 HPLC system (Thermo Scientific Dionex, Sunnyvale, California, USA) equipped with a BEH C8 analytical column (3 mm × 100 mm, 1.7 μm particle size) (Waters, Milford, Massachusetts, USA). The mobile phase, consisting of 0.1% formic acid (v:v) in acetonitrile (A) and water (B), was delivered at a flow rate of 0.4 mL/min employing the following gradient elution programme: 84% B for 2.0 min, 84–60% B from 2.0 to 12.0 min, 60–20% B from 12 to 15 min, 20–84% B from 15.0 to 17.0 min and hold 84% B for 5.0 min for column equilibration. An injection volume of 5 μL was used.

2.4.2. Mass spectrometry

Mass spectrometry detection was performed on a TSQ Quantum Ultra triple quadrupole mass spectrometer (Thermo Fisher Scientific, Waltham, Maryland, USA) equipped with a heated electrospray ionization interface (HESI II Probe) operating in the positive ion mode. Data acquisition and processing were accomplished using Xcalibur 2.1 software. The operating parameters for the mass spectrometer were as follows: vaporizer temperature: 234 °C, sheath gas pressure: 50 psi, aux gas pressure: 5 psi, spray voltage: 3500 V, capillary temperature: 400 °C.

To unquestionably identify and quantify each disaccharide, two ion transitions were monitored in selected reaction monitoring (SRM) mode. The SRM transitions for each disaccharide were chosen and optimized by the direct infusion of butanolysed standard solution into the mass spectrometer. Ion transitions selected for quantitative (Q3-quan) and qualitative (Q3-qual) analysis, together with retention times, tube lenses and collision energies, are shown in Table 1.

2.5. Method validation

The developed method was validated according to European Medicines Agency (EMA) [31] and Food and Drug Administration (FDA) [32] guidelines in terms of calibration range, intra- and inter-day accuracy, intra- and inter-day precision, matrix effect and stability.

Standard solutions of GAGs were prepared to cover a concentration range of calibration curves 0.05–80 μg/mL. Calibration curves for each GAG were constructed by plotting the ratio of the peak area of the analyte to that of the internal standard against concentration. The limit of detection (LOD) of each GAG was calculated from the concentrations with a signal-to-noise (S/N) ratio of 5. Linearity was evaluated by applying least-square regression. Intra-day accuracy and precision were carried out by measuring the three QC concentrations: 0.6 μg/mL – low QC (LQC), 40 μg/mL – medium QC (MQC) and 60 μg/mL – high QC (HQC) in five replicates on the same batch. Inter-day accuracy and precision were assessed by analyzing three sets of QC samples within three consecutive days, including five independent replicates of QC samples per level in each analytical run.

The method accuracy [%A] was calculated as the percent recovery using the following equation:

$$[\%A] = \frac{x_i}{\mu} \cdot 100$$

where: x_i–mean measured concentration, μ - nominal concentration;

whereas the precision [%RSD] of the method was evaluated as a percentage of relative standard deviation:

$$[\%RSD] = \frac{\delta}{x_i} \cdot 100$$

where: δ–standard deviation, x_i–mean measured concentration.

According to EMA and FDA guidelines, the method accuracy should be within 85–115%, and the method precision should not exceed 15%, except for the lowest concentration on the calibration curve.

The absolute matrix effects were evaluated as the variability of the response from lot to lot by analyzing 6 lots of plasma and urine, spiked at LQC and HQC standard solution.

The sample preparation process undermined the calculation of relative matrix effects. Thus, the alternative method (absolute matrix effect) included in the EMA guideline was used.

The stability of KS, CHS, HA and HS derivative disaccharides was assessed in artificial plasma and urine after 48 h storage at 10 °C, and after 7 days storage at −80 °C after the sample preparation process, including at least three independent replicates of QC samples per concentration. The stability was calculated as the accuracy based on a comparison of the detector response for QC samples analyzed immediately after preparation and after storage. The accuracy within 80–120% indicates that the analytes were stable under the studied conditions.

2.6. Demonstration of method applicability

2.6.1. In vitro investigations

The immortalized endothelial cells (EA.hy926, ATCC CRL-2922, Manassas, USA) were grown in Dulbecco's Modified Eagle's Medium (DMEM) containing 4.5 mg/mL glucose, 10% foetal bovine serum, 1% antibiotics (penicillin-streptomycin) and 2% HAT medium supplement and were maintained at 37 °C in an air atmosphere with 5% CO_2. For the experiments, the cells were seeded into 96-well plates at ca. 2×10^4 cells per well. After a 2-day-long incubation, the cell medium was removed, and 200 μL of fresh medium containing either individual enzymes or a mixture of enzymes (heparinase I, II, III, hyaluronidase and chondroitinase ABC) was added into wells. The final concentrations of the enzymes in individual experiments were: 3 or 300 mIU/mL for hyaluronidase; 0.03 or 3 mIU/mL for the other enzymes and in the mixture: 30 mIU/mL for hyaluronidase and 1 mIU/mL for the other enzymes. Stock solutions for all single enzymes were prepared in appropriate buffers, composition of which were provided by the supplier. The mixture of enzymes, was prepared in buffer pH 7.0, which was sufficient to maintain activity of all enzymes [33,34]. The controls were incubated with DMEM culture medium without enzymes. The cells were incubated for 1 h at 37 °C, after which time, the cell medium was siphoned off and then used for further analysis.

2.6.2. Atomic force microscope (AFM) analysis

The nanomechanical properties of the endothelial GLX were determined with an atomic force microscope (AFM)-based nano-indentation technique, as described previously [59]. Briefly, a triangular cantilever (Novascan Technologies, Boone, North Carolina, USA) with a mounted spherical tip (diameter 10 μm) and a nominal spring constant of 10 pN/nm indents the cells with a loading force of 0.5 nN. The reflection of a laser beam is used to quantify the cantilever deflection. By knowing the deflection sensitivity, cantilever force and piezo displacement, the stiffness [pN/nm] and thickness [nm] of the GLX can be calculated from the resulting force–distance curves using the Protein Unfolding and Nano-Indentation Analysis Software PUNIAS 3D version 1.0 release 2.2 (http://punias.voila.net).

EA.hy926 cells were grown to confluence prior to the start of the experiment. Cells were either treated with chondroitinase ABC, endo-β-galactosidase, heparinase I, heparinase III, a mixture of all or solvent for 1 h within the incubator before beginning the AFM measurements. GLX measurements on living cells were performed in HEPES-buffer (HEPES: 4-(2-hydroxyethyl)- 1-piperazineethanesulfonic acid; buffer: 140 mM NaCl, 5 mM KCl, 1 mM $CaCl_2$, 1 mM $MgCl_2$, 5 mM glucose, 10 mM HEPES) supplemented with 1% foetal bovine serum at 37 °C in a fluid chamber with a Nanoscope Multimode 8 AFM (JPK-Bruker, Berlin, Germany) JPK Nanowizard 4 AFM (JPK-Bruker, Berlin, Germany).

2.6.3. Creatinine measurements

Primary stock solutions of creatinine (1 mg/mL) and cimetidine (IS, 1 mg/mL) were prepared in water. Calibrators (1.25, 2.5, 5, 10, 25, 50, 100 and 250 μg/mL) were freshly prepared by the addition of different aliquots of the stock solution of the creatinine to water. Frozen urine samples were thawed to room temperature and briefly centrifuged to suspend any settled precipitate. Sample (10 μL) was diluted 10 x with artificial urine (without creatinine), and 10 μL of IS solution (10 μg/mL) was added. Then, 200 μL of acetonitrile was added, mixed for 5 min and then centrifuged at 7378×*g* for 10 min. Twenty μL of the supernatant was added to 80 μL of water, mixed and used for analysis. All samples were analyzed using an UltiMate 3000 HPLC system (Thermo Scientific) coupled with a TSQ Quantum Ultra mass spectrometer (Thermo Scientific).

2.6.4. In vivo investigations

The developed and validated method was applied for the assessment of the KS, CHS, HA and HS concentrations in murine plasma and urine collected from male C57BL/6 mice purchased from the Center of Experimental Medicine in Medical University of Bialystok (Bialystok, Poland). ApoE/LDLR$^{-/-}$ mice were obtained from the Department of Human Nutrition, University of Agriculture (Krakow, Poland). The blood was drawn from the right ventricle, and 10% K_2EDTA was added at a ratio of 1:60. All blood samples were centrifuged at 664×*g* for 12 min at 4 °C, and collected plasma was kept at −80 °C until GAG analysis.

To collect urine specimens, mice were individually placed in specially designed metabolic cages (Techniplast). After 12 h, urine samples were collected, clarified by centrifugation (10 000×*g*, 10 min) and stored at −80 °C for further measurements.

All procedures carried out on animals were performed according to EU Directive 2010/63/EU for animal experiments and were approved by the II Local Ethics Committee for Experiments on Animals in Krakow (approval number: 107/2020).

2.7. Data analysis

The statistical analysis of results and data visualization were performed using GraphPad Prism 7 software (La Jolla, CA, USA). After the assessment of normality of distribution and homogeneity of variance (Brown-Forsythe test), nonparametric (Kruskal–Wallis or Mann–Whitney *U* test) or parametric (one-way ANOVA with post hoc Dunnett's or Tukey's test or Student's t-test) tests were performed. Statistics were applied considering $p < 0.05$ as being statistically significant.

3. Results and discussion

3.1. MS-based assays for measuring GAG concentration; comparison of methanolysis and butanolysis-based derivatization

Many MS-based assays for measuring GAGs have been reported [26,35,36]. They can be roughly divided into two groups: the first based on enzymatic digestion and the second based on chemical digestion. Enzymatic digestion preserves complex information about the sulfation and acetylation sites of native GAGs. Unfortunately, the quantitation of all disaccharides of GAGs may, in fact, be impossible because of the availability and cost of disaccharide standards and the conditions essential for enzyme usage. Furthermore, the enzymatic digestions are time consuming, and bacterial lyases introduce a C4–C5 double bond into the nonreducing terminal hexuronate residue of a released disaccharide, leading to the loss of information on the absolute configuration of the carbonyl group. Chemical digestion is based on alcoholysis using, for example, methanol, 2-propanol and butanol. This strategy was designed to reduce the complexity of the GAG quantification, minimizing the intricacy of the polysaccharides by desulphation and depolymerization. Concurrently, the alkylation of GAGs based on alcoholysis improves the sensitivity of the method because after the depolymerization, the molar amount of disaccharide is significantly higher than the molar amount of the starting material. Despite the urgent need to understand GAGs' role, no one, to the best of our knowledge, has developed a method that could be used for the simultaneous quantification of all GAGs in a reliable manner [37].

Clearly, the analysis of chemically derived GAG products has limitations. It should be noted that the detection of GAG fragments is complex and does not provide an unquestionable estimation of the total GAGs in biological samples. However, currently, it is a promising method for determining the difference in GAG concentrations in biological fluids, and it can be a milestone in understanding the role of GLX in the progression of different diseases associated with endothelial dysfunction.

As documented earlier, methanolysis of GAGs followed by LC-MS/MS analysis has been successfully employed to determine the concentration of KS, CHS, HA and HS in a number of different biological samples. However, it has been shown that the methanolysis reaction does not occur completely over a practical time range [37,38]. This issue

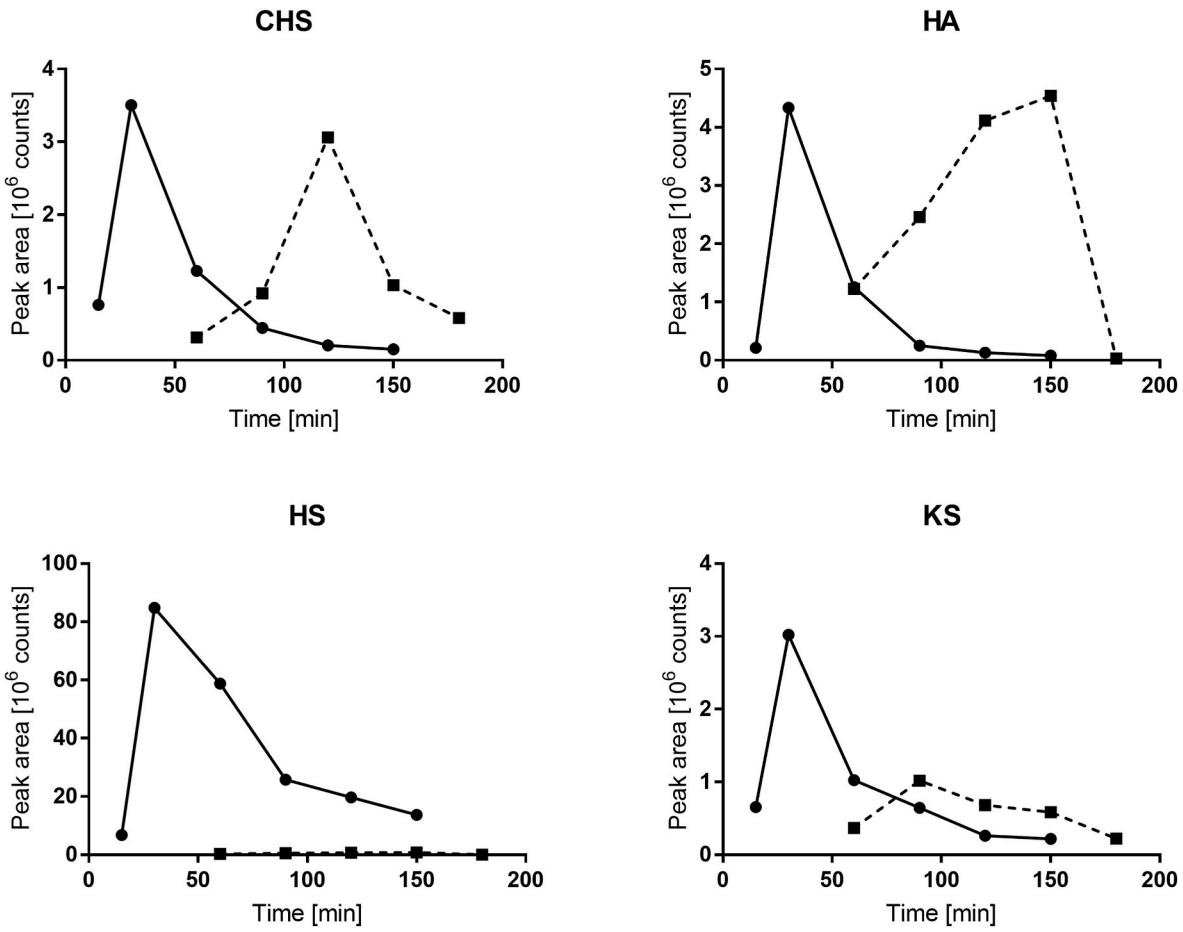

Fig. 1. Peak areas for the most abundant disaccharide products obtained from methanolysis at 65 °C (dotted line) or butanolysis at 100 °C (solid line) collected at various time intervals.

affected the accurate quantification, maximum yield and, consequently, signal intensity/sensitivity and directed the attention toward the use of longer-chain alcohols with higher boiling points, particularly butanol. To select the most suitable duration of the reaction, methanolysis and butanolysis were performed over a different time range. The reaction temperature conditions were chosen based on literature data, which showed that the most efficient digestion occurs at 100 °C for butanolysis and 65 °C for methanolysis. The peak areas of the most abundant peaks in a particular time during butanolysis and methanolysis are compared in Fig. 1. The resultant alkylated disaccharides are quantifiable by LC-SRM/MS. It was found that butanolysis progressed much more rapidly than methanolysis, with the peaks reaching maximum areas after approximately 30 min, and concurrently butanolysis was at least as sensitive as methanolysis; moreover, in the case of HS and KS, the obtained peak areas were about 100-fold larger, which is in line with previously published results. As it was earlier evidenced prolonged alcoholysis lead to degradation of disaccharides to monosaccharides. This explains why the peak area went down so dramatically after 30 min of incubation. The degradation of disaccharide to monosaccharide upon butanolysis was supported by time-dependent increase in butylated glucosamine in work of Trim et al. [37].

3.2. Characterization of GAG disaccharides after butanolysis using LC-SRM/MS

CHS, HS and HA possess highly similar chemical structures. After butanolysis, obtained disaccharides generate not only the same mass-to-charge ratio (m/z) of parent ions but also, after fragmentation, they deliver the same product ions. Therefore, the presumption that a particular parent ion corresponds to specific GAGs stated in previously published works [19–22] is highly simplified and ultimately may lead to incorrect result interpretation.

All abundant disaccharide products resulted from GAG butanolysis were fragmented. The most intense parent ion providing a reproducible signal response was m/z 468.2 and 394.4 for KS, and these were selected for further analysis. Other detected masses corresponded to sodium adducts with N-deacetylated disaccharides (m/z 490.2 and m/z 416.2 for KS), N-acetylated disaccharides (m/z 488.2 and m/z 414.2 for KS) and sodium adducts with N-acetylated disaccharides (m/z 510.2 and m/z 436.2 for KS). Chromatograms that illustrate the separation of N-deacetylated disaccharides (m/z 468.2 and m/z 394.2 for KS) obtained after butanolysis of all examined GAGs and selected corresponding mass spectra after fragmentation are shown in Fig. 2.

Multiple peaks were observed for the products of GAG alcoholysis reactions and, as previously documented, these are the result of the formation of different disaccharide stereoisomers [39]. However, in the case of CHS and HA, it is highly possible for disaccharides to be formed by breaking the bond between the glucosamine residue and the uronic acid moiety. We observed more than two main peaks on the chromatogram, and the geometry of the second bond was different than in HS—it was a 1 → 3 rather than a 1 → 4 bond. Nevertheless, that phenomena requires further studies. For the purposes of relative quantitation, for all analytes, one of the peaks based on the best separation and intensity was chosen and used for further quantitative analysis.

During the development of the method the variation in the formation of the individual derivatives of disaccharides were verified. The percentage variation of disaccharides after butanolysis of the same concentration of the standard of KS, HS, CHS or HA undergoing butanolysis

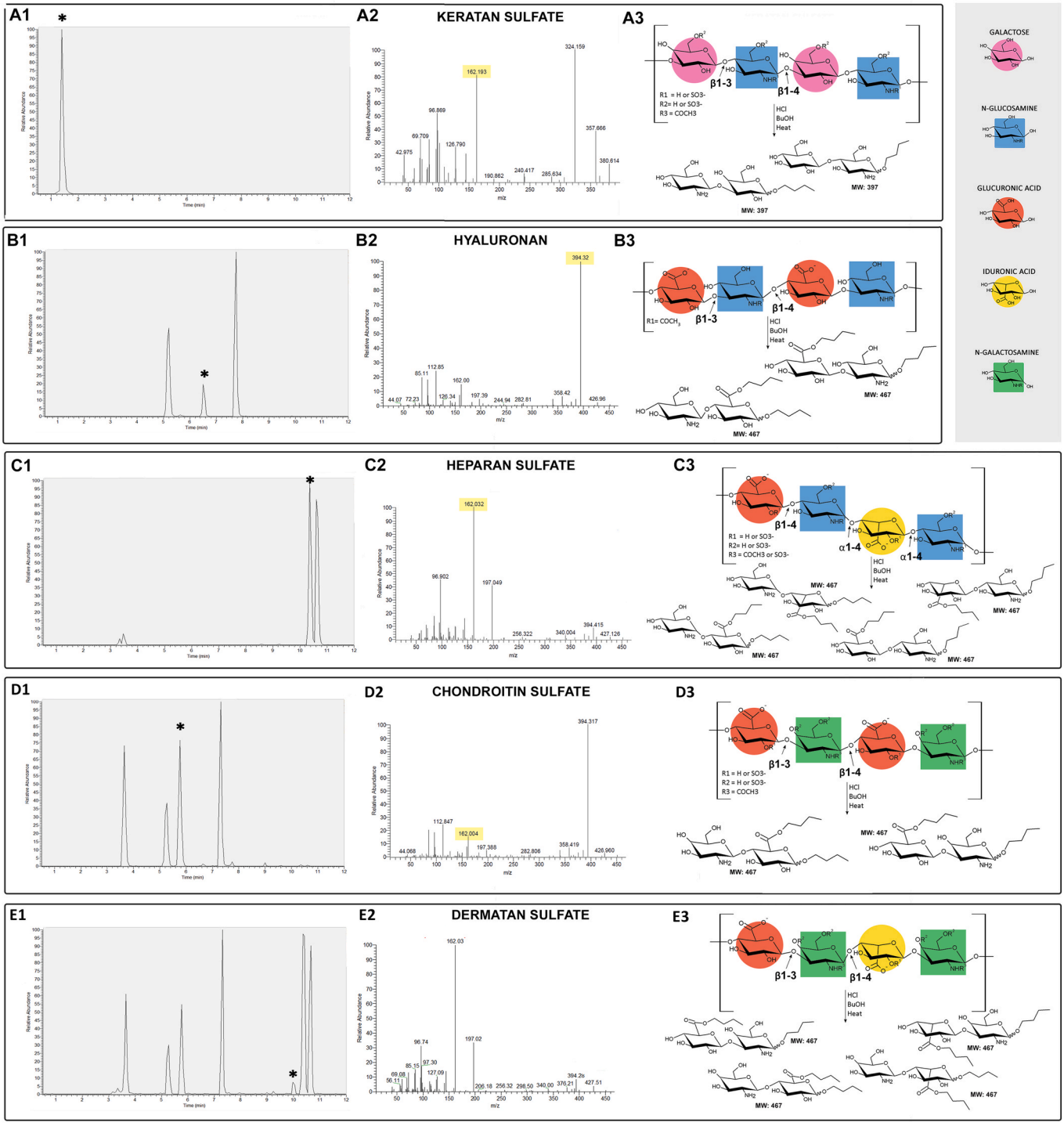

Fig. 2. Representative chromatograms for standard solutions of KS (A1), HA (B1), HS (C1), CHS (D1) and DS (E1) together with mass spectra for each of disaccharide products (A2-E2). Peaks marked with asterisks were used for quantification. Structures of studied GAGs together with proposed butanolysis products are showed in panels A3-E3. Butanolysis of GAGs provides desulphated, butylated disaccharides resulting from cleavage of glycosidic bonds.

under the same experimental conditions did not exceed ±15%.

The use of the BEH C8 column allowed for satisfactory chromatographic separation of formed disaccharides, in contrast to other tested columns, such as BEH C18 or BEH Amide.

There were substantial differences between the disaccharides in relative intensities of the fragment ions observed, which was used to finally confirm the origin of the peak. The main fragment ions observed were *m/z* 162 and *m/z* 394, consistent with the work of Trim et al. These disaccharides are primarily formed by the cleavage of the 1 → 4 glycosidic bond between the uronic acid and glucosamine residues in HS during alcoholysis [17]. Additionally, for each compound, the concentration calculated on the basis of the area of the remaining peaks was checked—the results did not differ by more than 15% (data not shown). Chromatograms presenting the separation of the mixture of all GAGs are depicted in Fig. 3.

Due to the fact that the only structural difference between CHS and DS is related to the presence of some IdoA in the latter, the pattern of disaccharides obtained after the butanolysis of DS was examined

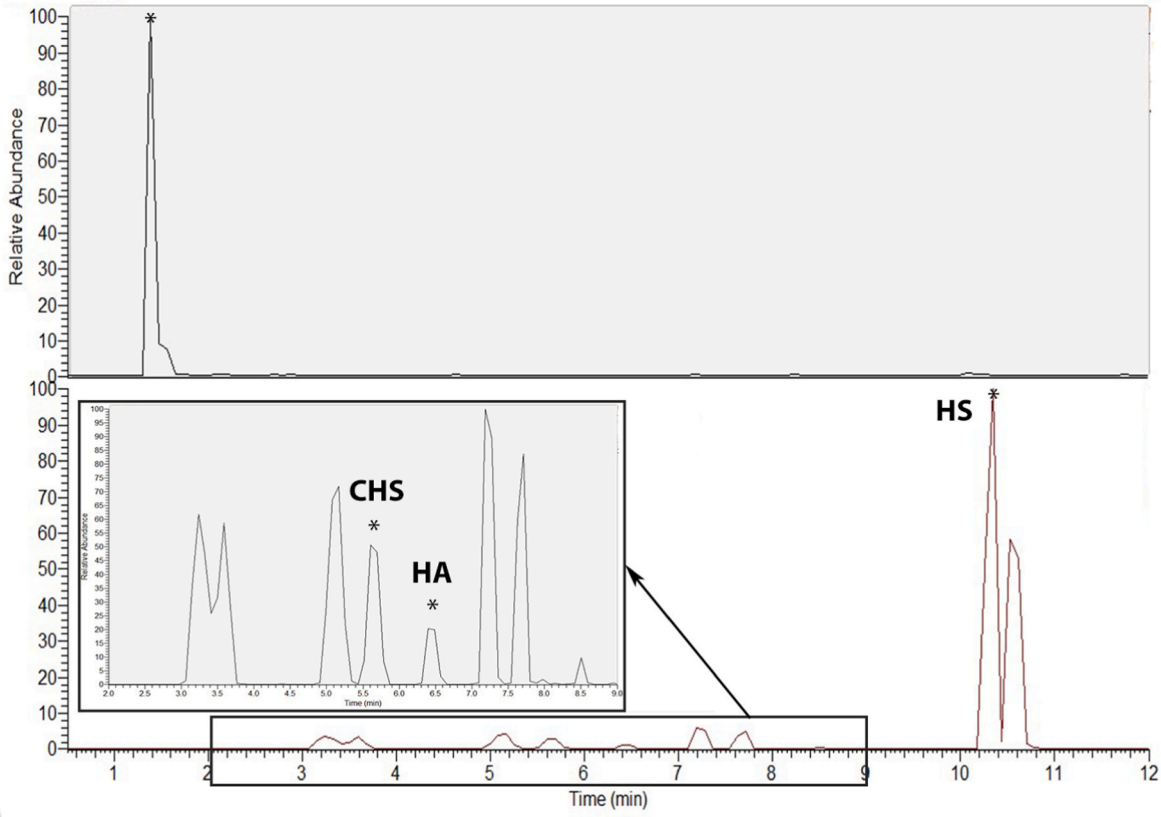

Fig. 3. Representative chromatograms of a mixture of GAG subunits. Upper panel shows peak for KS, lower panel shows peaks for HS, HA and CHS. Peaks marked with asterisks were used for quantification.

Table 2
Regression equations, determination coefficients (R^2) and LODs for studied GAGs in plasma and urine.

GAGs	Matrix	Linear range [μg/mL]	Regression equation	R^2	LOD [μg/mL]
KS	Plasma	0.1–80	Y = −9.59e-5+2.10e-3x	0.9905	0.05
	Urine	0.1–80	Y = −5.09e-4+1.12e-3x	0.9909	0.05
CHS	Plasma	0.1–80	Y = −8.62e-4+3.00e-3x	0.9936	0.05
	Urine	0.1–80	Y = −1.15e-3+3.38e-3x	0.9920	0.05
HA	Plasma	0.1–80	Y = −8.16e-4+1.78e-3x	0.9928	0.05
	Urine	0.1–80	Y = −1.07e-3+2.16e-3x	0.9975	0.05
HS	Plasma	0.05–80	Y = −3.25e-2+0.20x	0.9913	0.05
	Urine	0.05–80	Y = −3.53 e−3+0.22x	0.9928	0.05

carefully. As can be seen, the DS chromatogram appears to be similar to the combination of the HS and CHS chromatograms. Nevertheless, there is one peak that is characteristic for DS ($t_R = 9.99$). Our concern was that if DS occurred in samples, it can interfere with other GAGs and, furthermore, the validation of the method could not meet the criteria because of the same issue. However, there was no peak with $t_R = 9.99$ in any of the examined samples, either plasma or urine. Therefore, we assumed that DS occurs in biological matrices in such a small amount that we are not able to detect it, and we excluded DS from the panel of GAGs in the developed method. An analytical method that will allow DS determination without interfering with other GAGs will be a topic of further studies.

3.3. Method validation

Because GAGs are naturally occurring in biological samples, to eliminate the influence of endogenous components on the validated parameters, the calibration and quality control samples were prepared using artificial plasma and urine. The retention time was stable and reproducible for all analytes, both in artificial and murine biofluids.

3.3.1. Linearity

The calibration curves were plotted as the relationship between the peak area ratios of analyte/IS to the nominal concentration of the analyte. Because the deuterated internal standards for butylated disaccharides are not commercially available, metoprolol was used as an internal standard, given the fact that it possessed similar hydrophobic properties to the analytes under consideration. The validated method showed good linearity over the concentration range of 0.05–80 μg/mL for all compounds. All calibration samples were freshly prepared for each of three analytical runs. The best fit of standard curves for all analytes was obtained by applying a $1/x^2$ weighting algorithm. The range of calibration curves covered the expected concentration of all analytes in the studied biological fluids. The determination coefficients (R^2) were in the range of 0.9905–0.9975. The regression equations, R^2 and LODs for all studied compounds and matrices are presented in Table 2.

3.3.2. Accuracy and precision

The accuracy and precision of the method were estimated by including three concentration levels. All calculated parameters and

Table 3
Intra- and inter-day method accuracy and precision for GAGs in plasma.

GAGs	Concentration	Accuracy [%]		Precision [%]	
		Intra-day	Inter-day	Intra-day	Inter-day
KS	LQC	94.48	87.35	10.82	7.78
	MQC	101.99	96.72	7.63	9.10
	HQC	92.48	96.98	9.90	5.56
HS	LQC	101.18	100.89	12.38	9.63
	MQC	107.62	100.73	8.46	6.43
	HQC	101.50	96.04	9.13	5.02
CHS	LQC	88.54	93.81	7.68	10.59
	MQC	95.59	93.01	10.85	13.72
	HQC	91.33	96.82	12.26	5.25
HA	LQC	95.66	96.83	9.31	8.58
	MQC	100.43	94.08	5.72	6.36
	HQC	106.86	98.04	2.85	4.18

Table 4
Intra- and inter-day method accuracy and precision for GAGs in urine.

GAGs	Concentration	Accuracy [%]		Precision [%]	
		Intra-day	Inter-day	Intra-day	Inter-day
KS	LQC	114.91	106.36	14.25	11.72
	MQC	110.80	105.28	8.24	5.21
	HQC	113.26	104.71	8.48	7.40
HS	LQC	99.64	96.92	9.49	3.50
	MQC	106.96	106.45	9.90	5.50
	HQC	93.09	96.12	6.72	5.95
CHS	LQC	111.60	101.45	7.54	11.22
	MQC	112.81	110.72	8.28	2.12
	HQC	102.58	104.08	8.89	5.27
HA	LQC	86.79	95.26	2.49	9.18
	MQC	112.03	109.69	8.45	1.98
	HQC	112.63	108.97	3.35	3.56

Table 5
Analyte stability handled under various conditions.

GAGs	Concentration	Analyte stability			
		48 h [%]		7 days [%]	
		Plasma	Urine	Plasma	Urine
KS	LQC	112.57	103.61	95.41	103.40
	MQC	106.57	114.75	92.12	92.41
	HQC	113.65	107.4	96.99	93.66
HS	LQC	91.00	85.13	88.76	89.90
	MQC	97.17	94.48	87.41	112.41
	HQC	104.26	87.29	88.86	83.29
CHS	LQC	80.09	99.20	95.36	93.12
	MQC	102.40	100.13	95.81	90.69
	HQC	87.99	99.90	81.28	88.17
HA	LQC	98.49	111.71	86.52	83.85
	MQC	86.38	100.17	82.22	96.17
	HQC	93.50	106.36	85.17	90.47

Table 6
Matrix effect.

GAGs	Concentration	Matrix Effect [%]	
		Plasma	Urine
KS	LQC	5.74	4.82
	HQC	3.38	5.64
HS	LQC	5.59	7.42
	HQ	4.33	5.84
CHS	LQC	6.38	5.37
	HQC	4.94	2.86
HA	LQC	6.62	7.48
	HQC	3.96	6.33

assay conditions met the criteria of acceptance specified in FDA and EMA guidance. The intra-day accuracy for plasma and urine samples was within 88.54–107.62% and 86.79–114.91%, respectively. Inter-day accuracy for plasma and urine samples was within 87.35–100.89% and 95.26–110.72%, respectively. The intra-day method precision expressed as %RSD was below 12.38% (plasma) and 14.25% (urine). The inter-day precision was below 13.72% (plasma) and 11.72% (urine). The estimated values for method accuracy and precision are summarized in Table 3 and Table 4 for plasma and urine, respectively.

3.3.3. Stability

The stability of GAG disaccharides was calculated as the accuracy based on a comparison of the detector response for QC samples analyzed immediately after preparation and storage. The accuracy was within 82.22–114.75%, indicating the stability of analytes under the studied conditions. Obtained values are shown in Table 5.

3.3.4. Matrix effect

The matrix effect was in the range of 2.86–7.48%; thus, it fulfilled the specifications (<15%). Obtained values are provided in Table 6.

3.4. Method application

3.4.1. Evaluation of changes in GAG profiles in cell culture

Endothelial cells of the EA.hy926 lineage are a hybrid line created by the fusion of human umbilical vein endothelial (HUVEC) and A549 lung epithelial cancer [40] cells. The presence of GLX on the surface of these cells has previously been demonstrated by AFM [41]. The aim of the *in vitro* experiments conducted in this work was to determine the concentrations of individual components of the GLX produced by EA.hy926 cells and assess the changes in its structure after 1-h incubation with either the individual enzyme or the enzyme mixture that should decompose the long chains of GAGs.

First, we characterized the effects of an enzyme mixture at the concentrations previously described [33,42–46] on GAG release in EA.hy926 cells. In most publications, a mixture of at least 3 different enzymes was used, wherein the concentration of hyaluronidase in all cases is 50-fold higher than the concentration of other enzymes. Differences in the concentrations of individual GAGs released into the culture medium are shown in Fig. 4 (Panel A). Differences were statistically significant in the case of KS, HS and CHS. The lack of difference in the case of HA may be related to its looser binding to the GLX layer compared to other GAGs. The relative ratio of concentration between KS, HS, CHS, HA determined in the medium was similar to that determined in the plasma of mice, confirming the suitability of plasma for exploration of changes occurring in the structure of GLX. The statistical analysis was summarized in Table 7.

Then, we assessed the pattern of individual GAG release when the shedding of GLX was induced by various GAG-specific enzymes. The obtained results (Fig. 4 Panels: B1–B4) depict that heparinase I did not show significant activity in relation to HS produced by cells, whereas heparinase III exhibited concentration-related activity. Chondroitinase was found to be extremely active in both concentrations used, but no changes were observed in the hyaluronidase and endo-β-galactosidase-enriched samples. The lack of differences in the case of the endo-β-galactosidase, which was chosen as an enzyme specific to KS, could be attributed to inadequate concentration or nonoptimal reaction conditions.

3.4.2. AFM results

The atomic force microscope (AFM) was used here as a reference state-of-the-art method for the quantification of GLX nanomechanics on living endothelial cells. The quantification of GLX nanomechanical properties showed a softening of GLX after treatment with hyaluronidase by 22% (0.34 ± 0.02 pN/nm vs. control 0.44 ± 0.02 pN/nm; N = 3, n = 81–193) and by 38% after treatment with the enzyme mixture (0.26

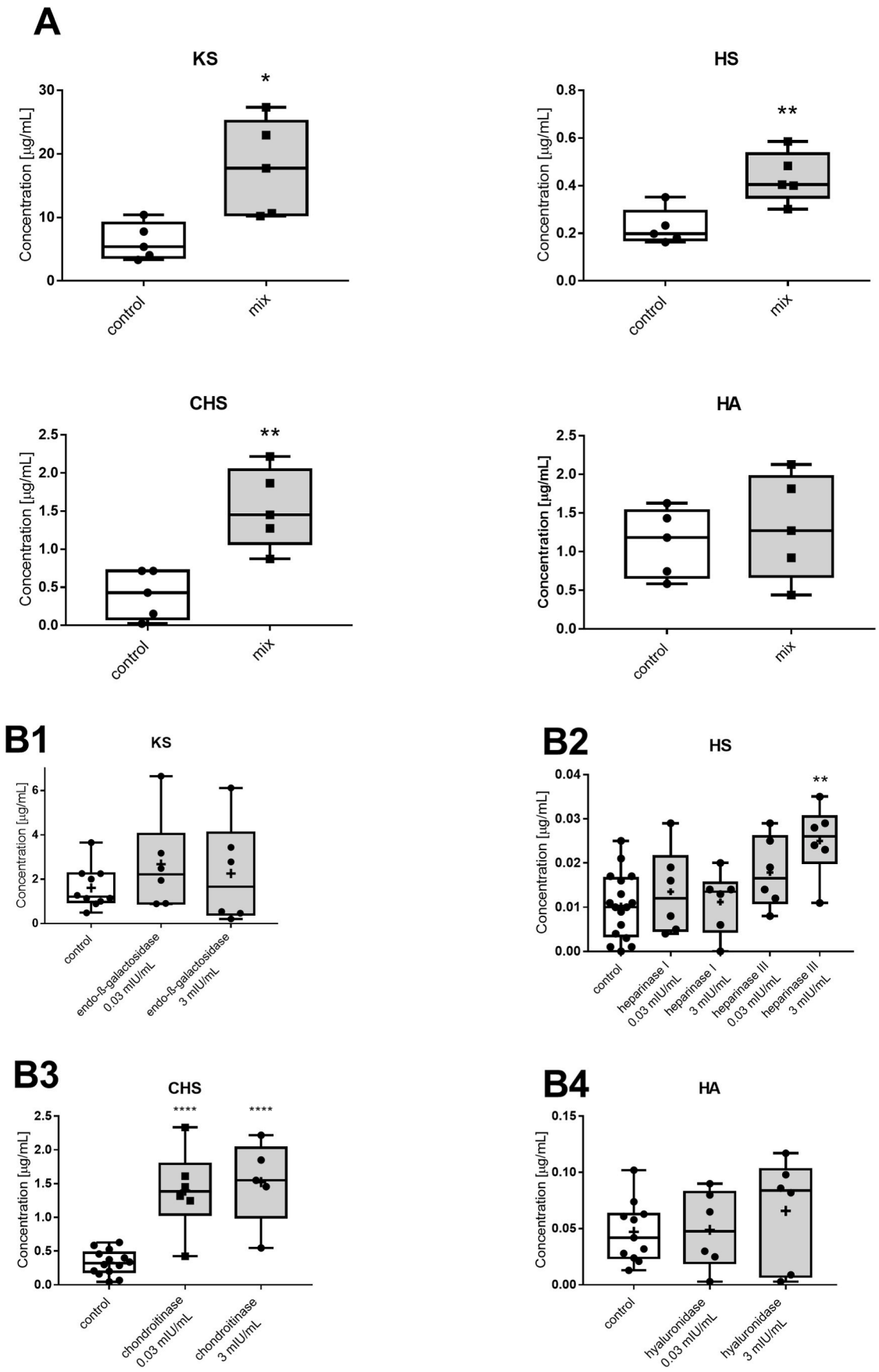

(caption on next page)

Fig. 4. Concentration of GAGs in culture medium after 1-h incubation of EA.hy926 cells with mixture of enzymes (mix), individual enzymes as compared with untreated cells (control). Concentration of KS, HS, CHS and HS in culture medium after 1-h incubation with mixture of enzymes (heparinase I, II, III, hyaluronidase and chondroitinase ABC) compared with untreated cells (control) (A). Concentration of KS in culture medium after 1-h incubation with endo-β-galactosidase in two different concentrations (0.03 and 3 mIU/mL) compared with control (B1). Concentration of HS in culture medium after 1-h incubation with either heparinase I or III in two different concentrations (0.03 and 3 mIU/mL) compared with control (B2). Concentration of CHS in culture medium after 1-h incubation with chondroitinase ABC in two different concentrations (0.03 and 3 mIU/mL) compared with control (B3).Concentration of HA in culture medium after 1-h incubation with hyaluronidase in two different concentrations (3 and 300 mIU/mL) compared with control (B4). Statistical significance of changes was tested by *t*-test, the Kruskal–Wallis test, followed by Dunn's post hoc test or by one-way ANOVA with post hoc Dunnett's test. Data were considered statistically significant at *p < 0.05, **p < 0.01, ***p < 0.005, ****p < 0.001.

Table 7
The statistical analysis of the differences in the concentrations of individual GAGs released into the culture medium. Statistical significance of changes was tested by *t*-test.

GAG	Group	mean	SEM	t	df	p
KS	Control	6.190	1.303	3.215	8	0.0123
	Mix	17.790	3.363			
HS	Control	0.226	0.034	3.602	8	0.007
	Mix	0.435	0.047			
CHS	Control	0.408	0.142	4.133	8	0.0033
	Mix	1.535	0.233			
HA	Control	1.115	0.198	0.5507	8	0.5969
	Mix	1.314	0.303			

± 0.01 pN/nm vs. control 0.44 ± 0.02 pN/nm; N = 3, n = 151–193). More importantly, GLX thickness was affected within all single enzyme treatments, with a reduction of GLX height as compared to the value of GLX thickness in untreated cells. Treatment with the enzyme mixture showed the most prominent impact, with a reduction of GLX by 43% (70.1 ± 1.7 nm vs. control 125.1 ± 3.8 nm; N = 3, n = 151–193). Differences in the nanomechanical properties and integrity of the GLX after enzyme treatment are shown in Fig. 5. The results obtained are consistent with previous reports [47]. It is worth noting that the AFM technique allows to assess only the physical parameters of the GLX without offering information on its accurate structure. Therefore, it can be stated that the exclusive reliance on AFM technique cannot offer a comprehensive image of the GLX or provide information about the biochemical nature of GLX disruption in contrast to biochemical analysis of GAG-derived products.

3.4.3. GAG profiles in plasma and urine in mice

Previously, GAG concentration was assessed in various matrices [39,48,49]. Here, we characterized GAG concentration in plasma and urine, most relevant to assessing systemic endothelial GLX degradation. Our results demonstrated that the major type of GAGs present in plasma was represented by KS, but in urine, this ratio was different, and the relative concentration of CHS was higher (Fig. 6). Due to the fact that GAGs are an obligatory constituent of the basal laminae in the urothelium, contributing to maintaining transmembrane permeability and preventing stone formation [50], we are tempted to speculate that the determination of GAG concentration in urine does not really reflect the GLX changes of systemic endothelium and may come, for example, from damaged bladder epithelium and other sources within the urinary tract. Therefore, systemic endothelial GLX could be best studied based on GAG concentration in plasma and would better reflect the endothelial GLX condition than GAGs in urine.

3.4.4. GAG pattern in plasma in ApoE/LDLR^{-}/$^{-}$ and wild-type mice

Despite the aforementioned limitations, the validated method was applied for the quantification of KS, CHS, HA and HS in plasma (Fig. 7) as well as in urine (Fig. 8) in ApoE/LDLR$^{-/-}$ and C57BL/6 mice. In the ApoE/LDLR$^{-/-}$ mice model, endothelial dysfunction precedes atherosclerotic plaque development, similar to how it occurs in humans [12]. Young (4-week-old) and old (40-week-old) control (C57BL/6) mice were used for comparison. We demonstrated previously that in 4- to 8-week-old ApoE/LDLR$^{-/-}$ mice at the stage proceeding development of the well-defined atherosclerosis, the dysfunctional phenotype of endothelium involved diminished glycocalyx coverage and length and both parameters of glycocalyx were further compromised in 28-week-old ApoE/LDLR$^{-/-}$ mice [12]. Here we used 4-week-old and 40-week-old ApoE/LDLR$^{-/-}$ mice mice, so we used two control groups of age-matched control mice (C57BL/6) to be able to determine whether the observed changes are related to ageing or atherosclerosis progression [51,52]. Earlier, it was demonstrated that the endothelial GLX on the luminal surface of the common carotid artery in ApoE/LDLR^{-}/$^{-}$ was significantly compromised compared to in C57BL/6 mice [53]. In analyzed plasma (and also urine) samples, the concentration of KS was particularly high (approximately 10 μg/mL), which is in agreement with the results obtained by Auray-Blais et al. [54]. HA and CHS exhibited lower levels as compared with KS, but still in around 1 μg/mL range, whereas HS was present at a much lower concentration in plasma (approximately 0.2 μg/mL). These results are thought provoking and seem contradictory to a common belief that KS has only a minor role in GLX. This situation might be due to the fact that HS and HA were measured most often as GAGs representative for GLX, not KS and CHS, as also measured here and only in some reports [54].

Interestingly, it seems to be a widely accepted view that HS is the most abundant GAG in GLX, accounting for 50–90% of the total GAG GLX pool, and it is typically present in a ratio of 4:1 with the second most common CHS [55–57]. This paradigm has arisen from the paper published in 1985 by Rapraeger A. et al., although the original data referred to the GAG concentration in epithelial rather than endothelial cells [58]. Our data suggest that KS is a major constituent of endothelial GLX as well as in plasma, suggesting a possible important structural and functional role of KS in GLX, which to the best of our knowledge, has not been appreciated previously.

Our results confirmed an age-dependent decline in GAG concentration in the plasma of C57BL/6 mice. This observation agrees with previous observations that show its globally reduced levels in older individuals and is also in agreement with our unpublished results showing that age-dependent endothelial dysfunction was already present at the age of 40 weeks in mice (A. Bar et al., 2021, unpublished). Of note in our work, all GAG-specific disaccharides detected in plasma, representative of KS-, HS-, CHS- and HA-constituents of GLX displayed an age-dependent decrease.

The important observation of this work was to show that in 4-week-old ApoE/LDLR$^{-/-}$ mice, at the stage of endothelial dysfunction but prior to atherosclerotic plaque development [12], the concentrations of CHS, HA and HS were similar to the control group, albeit that the KS plasma concentration was notably higher, suggesting that the KS-based detection of GLX integrity may prove more sensitive to detect early changes in GLX integrity in hypercholesterolemia and atherosclerosis. In our previous work, we demonstrated that in 4-week-old ApoE/LDLR$^{-/-}$ mice, GLX coverage was reduced and endothelial stiffness was increased, whereas GLX length was significantly decreased at the age of

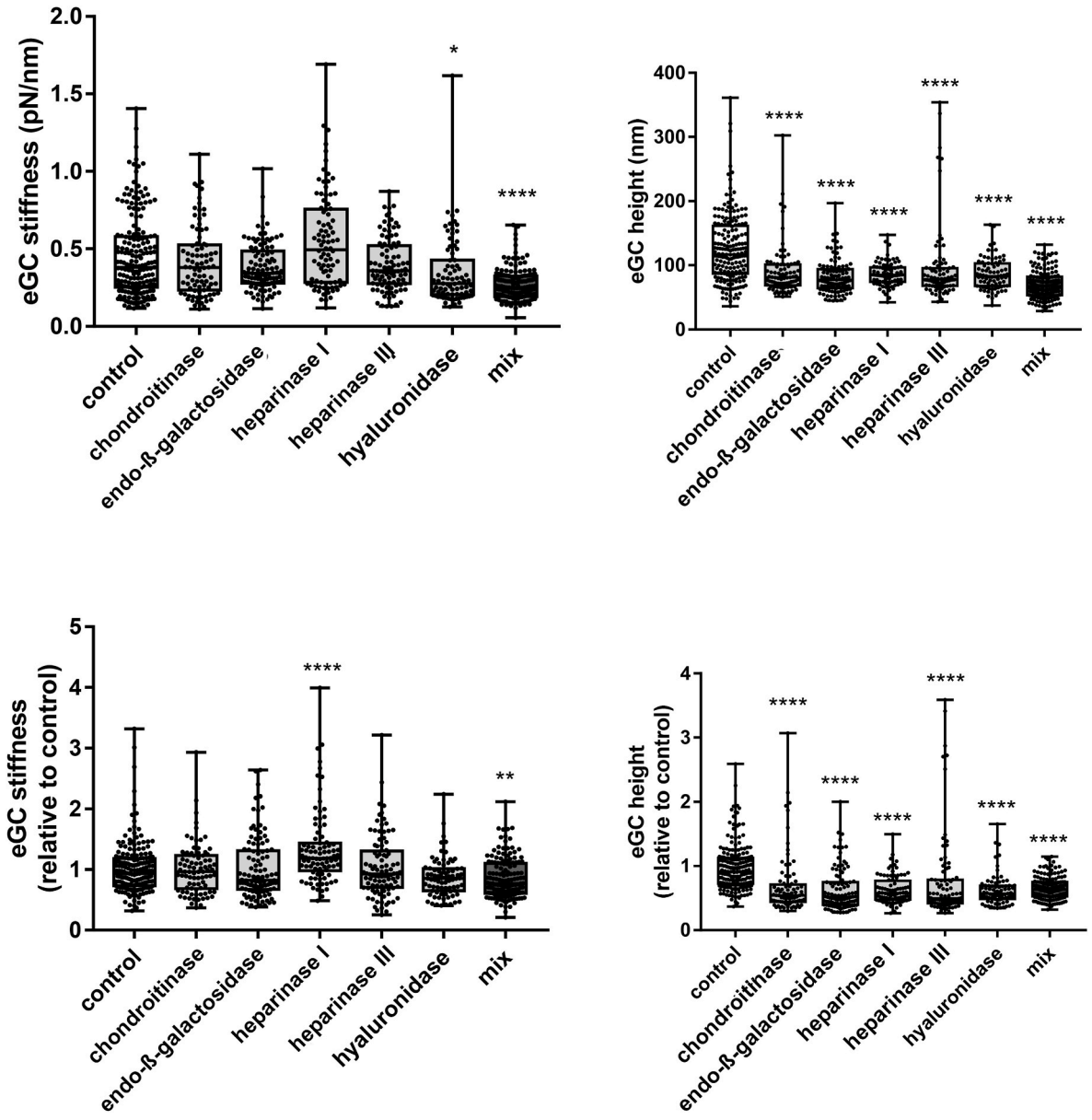

Fig. 5. Effects of 1-h incubation of EA.hy926 cells with 5 different enzymes or mixture of enzymes (mix) on the nanomechanical properties and integrity of the glycocalyx as compared with untreated cells. Using AFM measurements, the height and stiffness of the glycocalyx were determined. Statistical significance of changes was tested by one-way ANOVA with post hoc Dunnett's test. Data were considered statistically significant at *$p < 0.05$, **$p < 0.01$, ***$p < 0.005$, ****$p < 0.001$.

8 weeks [12]. In 40-week-old mice, at the stage of advanced atherosclerosis, the levels of concentrations of KS, HS and HA were still significantly elevated, demonstrating the further progression of pathological changes over time as compared with the age-dependent decline in plasma GAG concentration in C57BL/6 mice. Again, these results are compatible with our previous report showing that in 40-week old ApoE/LDLR$^{-/-}$ mice, there was a further reduction of GLX length and coverage with a concomitant further increase in endothelial permeability [12].

4. Conclusions

In the present work, we developed a novel method for the simultaneous quantification of selected GAGs by butanolysis-based derivatization and LC-SRM/MS for the assessment of GLX disruption *in vitro* and *in vivo*. Several crucial steps and advantages of the new approach have been presented when compared to previously published methods: increased assay sensitivity, faster reaction time of derivatization and better chromatographic characteristics in reversed-phase separations, providing the accurate identification and quantification of specific GAG-derived disaccharides. Using this method, we comprehensively characterized the loss of KS-, HS-, CHS- and HA-based constituents of GLX integrity in endothelial cells (EA.hy926) subjected to various GAG-degrading enzymes, and we also identified the profile of changes in KS-, HS-, CHS- and HA-based biomarkers *in vivo* in plasma in the association with age-dependent and hypercholesterolemia -dependent endothelial dysfunction in mice. Overall, the proposed LC-SRM/MS assay may constitute the basis for further analytical developments in

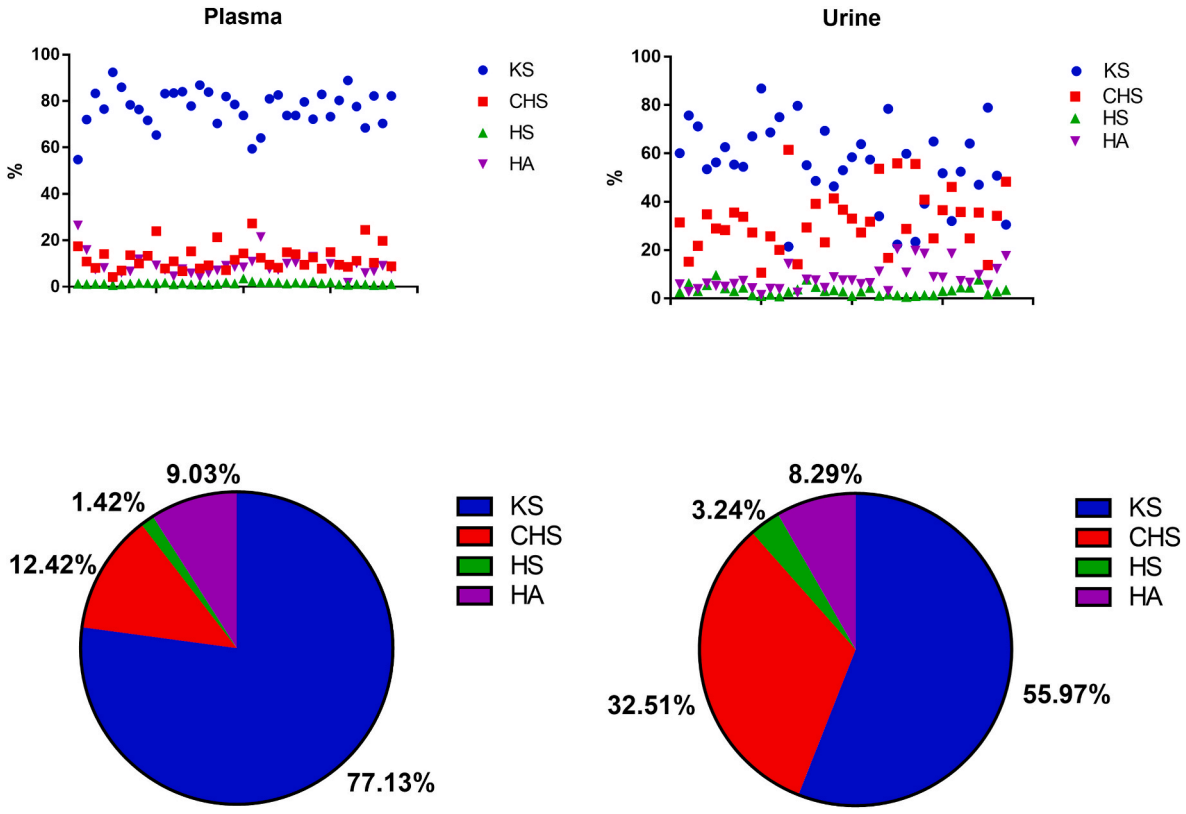

Fig. 6. Individual contribution of selected GAGs into total pool when murine plasma samples were compared against urine.

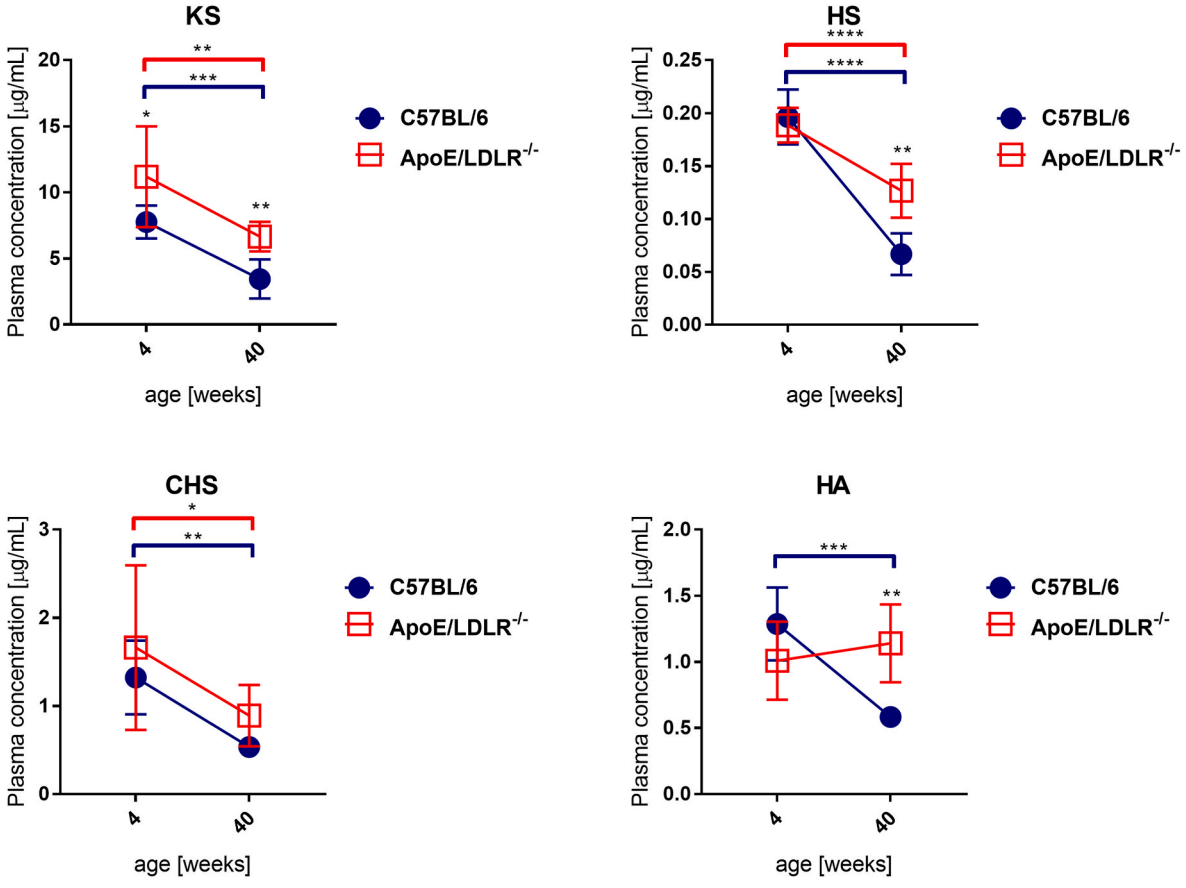

Fig. 7. Concentration of keratan sulphate (KS), heparin sulphate (HS), chondroitin sulphate (CHS) and hyaluronic acid (HA) in plasma of apolipoprotein E/low-density lipoprotein receptor-deficient (ApoE/LDLR−/−) mice at the age of 4 and 40 weeks in comparison to 4- and 40-week-old control C57BL/6 mice (n=8). Statistical significance was assessed by *t*-test, or the Kruskal–Wallis test, followed by Dunn's post hoc test. Data were considered statistically significant at *P < 0.05, **P < 0.01, ***P < 0.001, ****P < 0.0001.

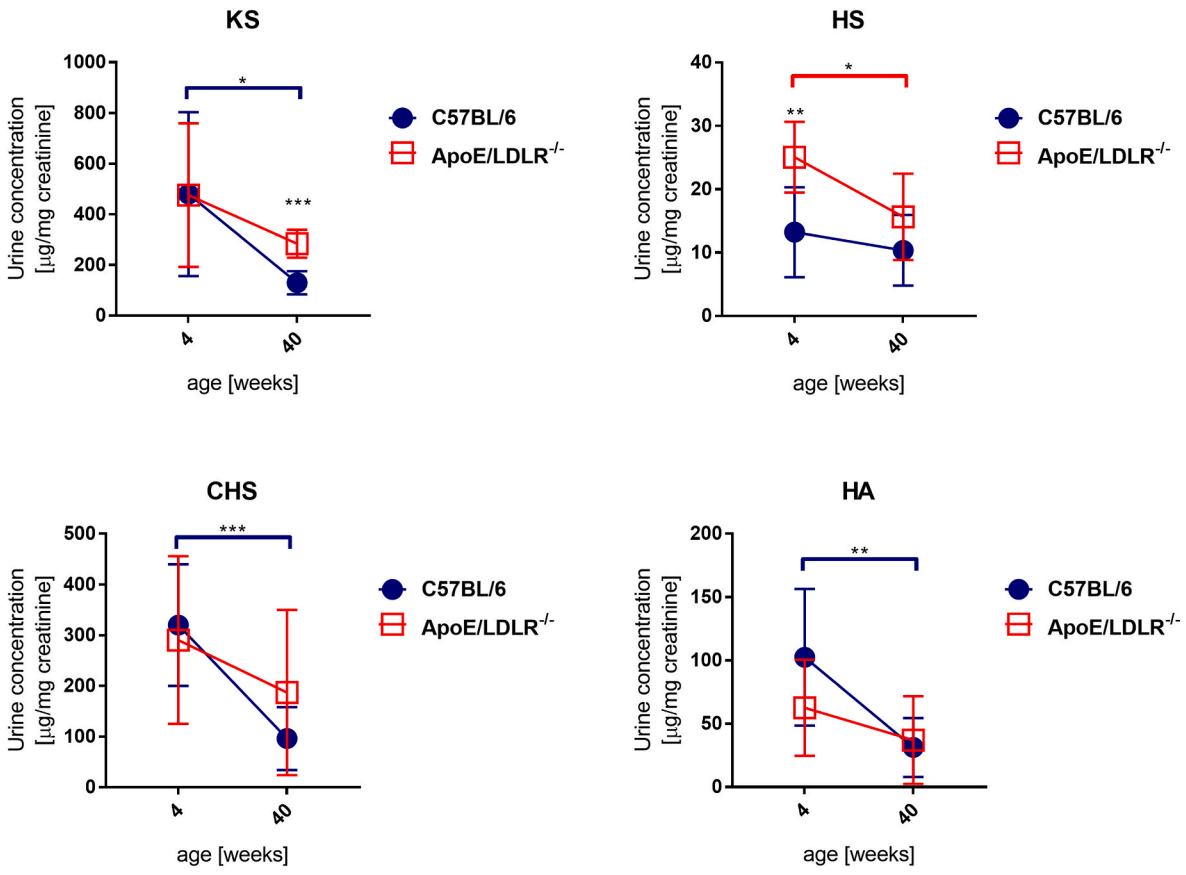

Fig. 8. Concentration of keratan sulphate (KS), heparin sulphate (HS), chondroitin sulphate (CHS) and hyaluronic acid (HA) in urine of apolipoprotein E/low-density lipoprotein receptor-deficient (ApoE/LDLR−/−) mice at the ages of 4 and 40 weeks in comparison to 4- and 40-week-old control, C57BL/6 mice (n=8). Statistical significance was assessed by *t*-test, or the Kruskal–Wallis test, followed by Dunn's post hoc test. Data were considered statistically significant at *P < 0.05, **P < 0.01, ***P < 0.001, ****P < 0.0001.

studies dedicated to evaluating the role of GLX integrity in endothelial biomedicine.

Author contributions

Karolina Matyjaszczyk-Gwarda: Methodology, Validation, Formal analysis, Investigation, Writing - Original Draft, writing final version of the manuscript. Agnieszka Kij: Methodology, Validation, Writing - Review & Editing, Mariola Olkowicz: Investigation, Writing - Review & Editing, Maria Walczak: Conceptualization, Writing - Review & Editing, Benedikt Fels: Methodology, Investigation, Kristina Kusche-Vihrog: Methodology, Investigation, Stefan Chlopicki: Conceptualization, Supervision, Writing - Review & Editing, writing final version of the manuscript.

Declaration of competing interest

The authors declare that they have no known competing financial interests or personal relationships that could have appeared to influence the work reported in this paper.

Acknowledgements

This work was supported by the National Science Centre, Poland [project PRELUDIUM 2018/31/N/NZ7/01528]. The authors would like to thank Krystyna Wandzel for her help in taking care of animals and Renata Budzynska for her assistance with cell line culture.

References

[1] I. Sieve, A.K. Münster-Kühnel, D. Hilfiker-Kleiner, Regulation and function of endothelial glycocalyx layer in vascular diseases, Vasc. Pharmacol. 100 (2018) 26–33, https://doi.org/10.1016/j.vph.2017.09.002.

[2] M. Walczak, J. Suraj, K. Kus, A. Kij, A. Zakrzewska, S. Chlopicki, Towards a comprehensive endothelial biomarkers profiling and endothelium-guided pharmacotherapy, Pharmacol. Rep. 67 (2015) 771–777, https://doi.org/10.1016/j.pharep.2015.06.008.

[3] A. Daiber, S. Chlopicki, Revisiting pharmacology of oxidative stress and endothelial dysfunction in cardiovascular disease: evidence for redox-based therapies, Free Radic. Biol. Med. 157 (2020) 15–37, https://doi.org/10.1016/j.freeradbiomed.2020.02.026.

[4] X. Zhang, D. Sun, J.W. Song, J. Zullo, M. Lipphardt, L. Coneh-Gould, M. S. Goligorsky, Endothelial cell dysfunction and glycocalyx - a vicious circle, Matrix Biol. 71–72 (2018) 421–431, https://doi.org/10.1016/j.matbio.2018.01.026.

[5] B.F. Becker, D. Chappell, M. Jacob, Endothelial glycocalyx and coronary vascular permeability: the fringe benefit, Basic Res. Cardiol. 105 (2010) 687–701, https://doi.org/10.1007/s00395-010-0118-z.

[6] A. Lukasz, C. Hillgruber, H. Oberleithner, K. Kusche-Vihrog, H. Pavenstädt, A. Rovas, B. Hesse, T. Goerge, P. Kümpers, Endothelial glycocalyx breakdown is mediated by angiopoietin-2, Cardiovasc. Res. 113 (2017) 671–680, https://doi.org/10.1093/cvr/cvx023.

[7] D.G. Warnock, K. Kusche-Vihrog, A. Tarjus, S. Sheng, H. Oberleithner, T. R. Kleyman, F. Jaisser, Blood pressure and amiloride-sensitive sodium channels in vascular and renal cells, Nat. Rev. Nephrol. 10 (2014) 146–157, https://doi.org/10.1038/nrneph.2013.275.

[8] S. Dogné, B. Flamion, N. Caron, Endothelial glycocalyx as a shield against diabetic vascular complications: involvement of hyaluronan and hyaluronidases, Arterioscler. Thromb. Vasc. Biol. 38 (2018) 1427–1439, https://doi.org/10.1161/ATVBAHA.118.310839.

[9] F.E. Curry, R.H. Adamson, Endothelial glycocalyx: permeability barrier and mechanosensor, Ann. Biomed. Eng. 40 (2012) 828–839, https://doi.org/10.1007/s10439-011-0429-8.

[10] U. Schött, C. Solomon, D. Fries, P. Bentzer, The endothelial glycocalyx and its disruption, protection and regeneration: a narrative review, Scand. J. Trauma Resuscitation Emerg. Med. 24 (2016) 48, https://doi.org/10.1186/s13049-016-0239-y.

[11] B. DellaValle, A. Manresa-Arraut, H. Hasseldam, A. Stensballe, J. Rungby, A. Larsen, C. Hempel, Detection of glycan shedding in the blood: new class of multiple sclerosis biomarkers? Front. Immunol. 9 (2018) 1–9, https://doi.org/10.3389/fimmu.2018.01254.

[12] A. Bar, M. Targosz-Korecka, J. Suraj, B. Proniewski, A. Jasztal, B. Marczyk, M. Sternak, M. Przybyło, A. Kurpińska, M. Walczak, R.B. Kostogrys, M. Szymonski, S. Chlopicki, Degradation of glycocalyx and multiple manifestations of endothelial dysfunction coincide in the early phase of endothelial dysfunction before atherosclerotic plaque development in apolipoprotein E/Low-Density lipoprotein receptor-deficient mice, J. Am. Heart Assoc. 8 (2019), https://doi.org/10.1161/JAHA.118.011171.

[13] A. Nelson, I. Berkestedt, A. Schmidtchen, L. Ljunggren, M. Bodelsson, Increased levels of glycosaminoglycans during septic shock, Shock 30 (2008) 623–627, https://doi.org/10.1097/SHK.0b013e3181777da3.

[14] R. Uchimido, E.P. Schmidt, N.I. Shapiro, The glycocalyx: a novel diagnostic and therapeutic target in sepsis, Crit. Care 23 (2019) 1–12, https://doi.org/10.1186/s13054-018-2292-6.

[15] I. Menkovic, A.S. Marchand, M. Boutin, C. Auray-Blais, Neonatal mass urine screening approach for early detection of mucopolysaccharidoses by UPLC-MS/MS, Diagnostics 9 (2019) 6–15, https://doi.org/10.3390/diagnostics9040195.

[16] B. DellaValle, H. Hasseldam, F.F. Johansen, H.K. Iversen, J. Rungby, C. Hempel, Multiple soluble components of the glycocalyx are increased in patient plasma after ischemic stroke, Stroke 50 (2019) 2948–2951, https://doi.org/10.1161/STROKEAHA.119.025953.

[17] E. Rahbar, J.C. Cardenas, G. Baimukanova, B. Usadi, R. Bruhn, S. Pati, S. R. Ostrowski, P.I. Johansson, J.B. Holcomb, C.E. Wade, Endothelial glycocalyx shedding and vascular permeability in severely injured trauma patients, J. Transl. Med. 13 (2015) 1–7, https://doi.org/10.1186/s12967-015-0481-5.

[18] S.R. Potje, T.J. Costa, T.F.C. Fraga-Silva, R.B. Martins, M.N. Benatti, C.E.L. Almado, K.S.G. de Sá, V.L.D. Bonato, E. Arruda, P. Louzada-Junior, R.D.R. Oliveira, D. S. Zamboni, C. Becari, M. Auxiliadora-Martins, R.C. Tostes, Heparin prevents in vitro glycocalyx shedding induced by plasma from COVID-19 patients, Life Sci. 276 (2021), https://doi.org/10.1016/j.lfs.2021.119376.

[19] W. Li, W. Wang, Structural alteration of the endothelial glycocalyx: contribution of the actin cytoskeleton, Biomech. Model. Mechanobiol. 17 (2018) 147–158, https://doi.org/10.1007/s10237-017-0950-2.

[20] Z. Shriver, I. Capila, G. Venkataraman, R. Sasisekharan, Heparin and heparan sulfate: analyzing structure and microheterogeneity, Handb. Exp. Pharmacol. 207 (2012) 159–176, https://doi.org/10.1007/978-3-642-23056-1_8.

[21] J.M. Trowbridge, R.L. Gallo, Dermatan sulfate: new functions from an old glycosaminoglycan, Glycobiology 12 (2002) 117R–125R, https://doi.org/10.1093/glycob/cwf066.

[22] K. Sugahara, T. Mikami, T. Uyama, S. Mizuguchi, K. Nomura, H. Kitagawa, Recent advances in the structural biology of chondroitin sulfate and dermatan sulfate, Curr. Opin. Struct. Biol. 13 (2003) 612–620, https://doi.org/10.1016/j.sbi.2003.09.011.

[23] I. Hargittai, M. Hargittai, Molecular structure of hyaluronan: an introduction, Struct. Chem. 19 (2008) 697–717, https://doi.org/10.1007/s11224-008-9370-3.

[24] B. Caterson, J. Melrose, Keratan sulfate, a complex glycosaminoglycan with unique functional capability, Glycobiology 28 (2018) 182–206, https://doi.org/10.1093/glycob/cwy003.

[25] B. DellaValle, H. Hasseldam, F.F. Johansen, H.K. Iversen, J. Rungby, C. Hempel, Multiple soluble components of the glycocalyx are increased in patient plasma after ischemic stroke, Stroke 50 (2019) 2948–2951, https://doi.org/10.1161/STROKEAHA.119.025953.

[26] F. Kubaski, H. Osago, R.W. Mason, S. Yamaguchi, H. Kobayashi, M. Tsuchiya, T. Orii, S. Tomatsu, Glycosaminoglycans detection methods: applications of mass spectrometry, Mol. Genet. Metabol. 120 (2017) 67–77, https://doi.org/10.1016/j.ymgme.2016.09.005.

[27] G. Gray, P. Claridge, L. Jenkinson, A. Green, Quantitation of urinary glycosaminoglycans using dimethylene blue as a screening technique for the diagnosis of mucopolysaccharidoses: an evaluation, Ann. Clin. Biochem. 44 (2007) 360–363, https://doi.org/10.1258/000456307780945688.

[28] J.R. Alonso-Fernández, J. Fidalgo, C. Colón, Neonatal screening for mucopolysaccharidoses by determination of glycosaminoglycans in the eluate of urine-impregnated paper: preliminary results of an improved DMB-based procedure, J. Clin. Lab. Anal. 24 (2010) 149–153, https://doi.org/10.1002/jcla.20375.

[29] C. Auray-Blais, P. Lavoie, H. Zhang, R. Gagnon, J.T.R. Clarke, B. Maranda, S. P. Young, Y. An, D.S. Millington, An improved method for glycosaminoglycan analysis by LC-MS/MS of urine samples collected on filter paper, Clin. Chim. Acta 413 (2012) 771–778, https://doi.org/10.1016/j.cca.2012.01.012.

[30] W. Christie, Preparation of ester derivatives of fatty acids for chromatographic analysis esters, in: W.W. Christie (Ed.), Adv. Lipid Methodol. – Two, Oily Press, Dundee, 1993, pp. 69–111, https://doi.org/10.1016/0009-3084(94)02308-5.

[31] European Medicines Agency (EMA), Guideline on bioanalytical method validation, Comm. Med. Prod. Hum. Use Guidel. EMEA/CHMP/ (2011).

[32] Food and Drug Administration (FDA), Bioanalytical Method Validation Guidance for Industry, 2018. https://www.fda.gov/files/drugs/published/Bioanalytical-Method-Validation-Guidance-for-Industry.pdf.

[33] G. Offeddu, C. Hajal, C. Foley, Z. Wan, L. Ibrahim, M.F. Coughlin, R.D. Kamm, Glycocalyx-mediated vascular dissemination of circulating tumor cells, BioRxiv (2020), https://doi.org/10.1101/2020.04.28.066746.

[34] T. Oguma, S. Tomatsu, A.M. Montano, O. Okazaki, Analytical method for the determination of disaccharides derived from keratan, heparan, and dermatan sulfates in human serum and plasma by high-performance liquid chromatography/turbo ionspray ionization tandem mass spectrometry, Anal. Biochem. 368 (2007) 79–86, https://doi.org/10.1016/j.ab.2007.05.016.

[35] S. Tomatsu, T. Shimada, R. Mason, A. Montaño, J. Kelly, W. LaMarr, F. Kubaski, R. Giugliani, A. Guha, E. Yasuda, W. Mackenzie, S. Yamaguchi, Y. Suzuki, T. Orii, Establishment of glycosaminoglycan assays for mucopolysaccharidoses, Metabolites 4 (2014) 655–679, https://doi.org/10.3390/metabo4030655.

[36] S.A. Khan, R.W. Mason, H. Kobayashi, S. Yamaguchi, S. Tomatsu, Advances in glycosaminoglycan detection, Mol. Genet. Metabol. 130 (2020) 101–109, https://doi.org/10.1016/j.ymgme.2020.03.004.

[37] P.J. Trim, J.J. Hopwood, M.F. Snel, Butanolysis derivatization: improved sensitivity in LC-MS/MS quantitation of heparan sulfate in urine from mucopolysaccharidosis patients, Anal. Chem. 87 (2015) 9243–9250, https://doi.org/10.1021/acs.analchem.5b01743.

[38] R.J. Linhardt, Analysis of glycosaminoglycans with polysaccharide lyases, Curr. Protoc. Mol. Biol. (1999), https://doi.org/10.1373/clinchem.2010.161141, 17.13B.1–16.

[39] P.J. Trim, A.A. Lau, J.J. Hopwood, M.F. Snel, A simple method for early age phenotype confirmation using toe tissue from a mouse model of MPS IIIA, Rapid Commun. Mass Spectrom. 28 (2014) 933–938, https://doi.org/10.1002/rcm.6861.

[40] C.J.S. Edgell, C.C. McDonald, J.B. Graham, Permanent cell line expressing human factor VIII-related antigen established by hybridization, Proc. Natl. Acad. Sci. U.S. A. (1983), https://doi.org/10.1073/pnas.80.12.3734.

[41] H. Oberleithner, W. Peters, K. Kusche-Vihrog, S. Korte, H. Schillers, K. Kliche, K. Oberleithner, Salt overload damages the glycocalyx sodium barrier of vascular endothelium, Pflugers Arch. Eur. J. Physiol. (2011), https://doi.org/10.1007/s00424-011-0999-1.

[42] K.K. McDonald, S. Cooper, L. Danielzak, R.L. Leask, Glycocalyx degradation induces a proinflammatory phenotype and increased leukocyte adhesion in cultured endothelial cells under flow, PLoS One (2016), https://doi.org/10.1371/journal.pone.0167576.

[43] Y. Zeng, E.E. Ebong, B.M. Fu, J.M. Tarbell, The structural stability of the endothelial glycocalyx after enzymatic removal of glycosaminoglycans, PLoS One (2012), https://doi.org/10.1371/journal.pone.0043168.

[44] R. O'Callaghan, K.M. Job, R.O. Dull, V. Hlady, Stiffness and heterogeneity of the pulmonary endothelial glycocalyx measured by atomic force microscopy, Am. J. Physiol. Lung Cell Mol. Physiol. (2011), https://doi.org/10.1152/ajplung.00342.2010.

[45] M.Y. Pahakis, J.R. Kosky, R.O. Dull, J.M. Tarbell, The role of endothelial glycocalyx components in mechanotransduction of fluid shear stress, Biochem. Biophys. Res. Commun. (2007), https://doi.org/10.1016/j.bbrc.2007.01.137.

[46] A. Wiesinger, W. Peters, D. Chappell, D. Kentrup, S. Reuter, H. Pavenstadt, H. Oberleithner, P. Kumpers, Nanomechanics of the endothelial glycocalyx in experimental sepsis, PLoS One 8 (2013) 1–14, https://doi.org/10.1371/journal.pone.0080905.

[47] Z.C. Cosgun, B. Fels, K. Kusche-Vihrog, Nanomechanics of the endothelial glycocalyx: from structure to function, Am. J. Pathol. 190 (2020) 732–741, https://doi.org/10.1016/j.ajpath.2019.07.021.

[48] C.-K. Chuang, H.-Y. Lin, T.-J. Wang, C.-C. Tsai, H.-L. Liu, S.-P. Lin, A modified liquid chromatography/tandem mass spectrometry method for predominant disaccharide units of urinary glycosaminoglycans in patients with mucopolysaccharidoses, Orphanet J. Rare Dis. 9 (2014) 135, https://doi.org/10.1186/s13023-014-0135-3.

[49] H. Zhang, S.P. Young, C. Auray-Blais, P.J. Orchard, J. Tolar, D.S. Millington, Analysis of glycosaminoglycans in cerebrospinal fluid from patients with mucopolysaccharidoses by isotope-dilution ultra-performance liquid chromatography - tandem mass spectrometry, Clin. Chem. 57 (2011) 1005–1012, https://doi.org/10.1373/clinchem.2010.161141.

[50] P. Ferrara, D. Rigante, S. Lambert-Gardini, E. Salvaggio, R. Ricci, M.L. Chiozza, D. Antuzzi, Urinary excretion of glycosaminoglycans in patients with isolated nocturnal enuresis or combined with diurnal incontinence, BJU Int. 86 (2000) 824–825, https://doi.org/10.1046/j.1464-410X.2000.00905.x.

[51] K.B. Komosińska-Vassev, K. Winsz-Szczotka, K. Kuznik-Trocha, P. Olczyk, K. Olczyk, Age-related changes of plasma glycosaminoglycans, Clin. Chem. Lab. Med. 46 (2008) 219–224, https://doi.org/10.1515/CCLM.2008.048.

[52] H. Zhang, T. Wood, S.P. Young, D.S. Millington, A straightforward, quantitative ultra-performance liquid chromatography-tandem mass spectrometric method for heparan sulfate, dermatan sulfate and chondroitin sulfate in urine: an improved clinical screening test for the mucopolysaccharidoses, Mol. Genet. Metabol. 114 (2015) 123–128, https://doi.org/10.1016/j.ymgme.2014.09.009.

[53] B.M. Van Den Berg, J.A.E. Spaan, T.M. Rolf, H. Vink, V. Den Berg, M. Bernard, J.A. E. Spaan, T.M. Rolf, Atherogenic region and diet diminish glycocalyx dimension and increase intima-to-media ratios at murine carotid artery bifurcation, Am. J. Physiol. Heart Circ. Physiol. 290 (2005) 915–920, https://doi.org/10.1152/ajpheart.00051.2005.

[54] C. Auray-Blais, P. Lavoie, B. Maranda, M. Boutin, Evaluation of urinary keratan sulfate disaccharides in MPS IVA patients using UPLC-MS/MS, Bioanalysis 8 (2016) 179–191, https://doi.org/10.4155/bio.15.239.

[55] H. Kolářová, B. Ambrůzová, L. Švihálková Šindlerová, A. Klinke, L. Kubala, Modulation of endothelial glycocalyx structure under inflammatory conditions, Mediat. Inflamm. (2014), https://doi.org/10.1155/2014/694312, 2014.

[56] S. Reitsma, D.W. Slaaf, H. Vink, M.A.M.J. Van Zandvoort, M.G.A. Oude Egbrink, The endothelial glycocalyx: composition, functions, and visualization, Pflugers Arch. Eur. J. Physiol. 454 (2007) 345–359, https://doi.org/10.1007/s00424-007-0212-8.

[57] A.R. Pries, T.W. Secomb, P. Gaehtgens, The endothelial surface layer, Pflügers Arch. - Eur. J. Physiol. 440 (2000) 653–666, https://doi.org/10.1007/s004240000307.
[58] A. Rapraeger, M. Jalkanen, E. Endo, J. Koda, M. Bernfield, The cell surface proteoglycan from mouse mammary epithelial cells bears chondroitin sulfate and heparan sulfate glycosaminoglycans, J. Biol. Chem. 260 (1985) 11046–11052.
[59] H Oberleithner, W Peters, K Kusche-Vihrog, S Korte, H Schillers, K Kliche, K Oberleithner, Salt overload damages the glycocalyx sodium barrier of vascular endothelium, Pflugers Archiv : Eur. J. Physiol. 462 (4) (2011) 519–528, https://doi.org/10.1007/s00424-011-0999-1.